Electron-positron momentum density in diamond, Si, and Ge

B. K. Panda, S. Fung, and C. D. Beling

Department of Physics, The University of Hong Kong, Hong Kong

(Received 14 June 1995)

The electron-positron momentum densities in diamond, Si, and Ge are calculated using a first-principles method. Comparison of the theoretical momentum densities with the experiment shows that the electron-positron correlation effects are very important in Si and Ge, while this effect is negligible in diamond because the electrons are tightly bound. Our analysis shows that only the upper two bands, which consist of the sp^3 hybridized orbitals, contribute to the structures at the low-momentum region of the momentum density. Diamond does not show these structures at the low-momentum region is due to its smaller lattice constant and weak electron-positron correlation effects.

I. INTRODUCTION

Diamond, Si, and Ge all have a diamond lattice structure as a result of the sp^3 hybrid orbitals forming tetrahedral bonding patterns which match the symmetry found in the diamond structure. It is observed that diamond has the largest band gap, and that this gap narrows from diamond to silicon to germanium, and finally vanishes for tin, exhibiting a metallic nature. This happens because the heavier the element the more energy is required to promote an atom from the ground state, the s^2p^2 configuration, to the bonding, sp^3, configuration.[1]

The angular correlation of positron annihilation radiations (ACPAR) is a powerful method for studying the electronic structure of solids,[2] because the positron mainly samples the valence electrons. In particular this technique is helpful in studying the covalent bonding features in diamond, Si, and Ge because the sp^3 orbitals are mainly distributed in the bond region. The electron momentum distributions along various crystallographic directions in Si and Ge have been studied by a number of researchers from the early stage of the application of the one-dimensional (1D) ACPAR measurements.[3–6] Apart from a few differences among the data of several groups, the overall shape of the momentum distributions in Si and Ge are found to be the same. The common features seen are (i) the momentum distributions are highly anisotropic in different crystallographic directions, (ii) there are temperature-dependent valleys along [100] and [110] directions and a hill along the [111] direction, and (iii) there are humps at the high-momentum region along [110] and [111] directions. Subsequent two-dimensional (2D) ACPAR measurements in Si and Ge by several groups[7–9] have confirmed the above findings. In general the three-dimensional momentum density is very successfully reconstructed from the two-dimensional ACPAR data, and shows many fine structures compared to that obtained from 1D and 2D ACPAR data. It is observed that the main features in ACPAR and momentum density data in Si and Ge are almost the same, and can be interpreted in a similar way. However, the momentum distributions in diamond are quite different from those in Si and Ge. The valleys and peaks in the low-momentum region of the momentum distributions, which are

so clearly seen in Si and Ge, have vanished in the case of diamond.[9]

In the late sixties Erskine and McGervey experimented with the nearly-free-electron model to explain the structure of the momentum distributions in Si and Ge.[4] This model does not take the bonding features or the orbitals, but correctly samples the **k** dependence by taking the area of the Jones zone along different crystallographic directions. With this simple model some of the features in the momentum distributions are reproduced and ascribed to the polyhedral shape of the Jones zone. However, this model could not account for the features in the low- and high-momentum regions of the momentum distributions. Moreover, the first 2D ACPAR data on Ge showed that the momentum distributions strongly deviated from the simple Jones zone picture, indicating that the success of this model in the 1D ACPAR results was largely a result of averaging in integration. However, Liu, Berko, and Mills, using the 2D ACPAR while observing the same marked discrepancy for Ge, have found good agreement with the Jones zone symmetry in diamond.

Stroud and Ehrenreich were the first in the late sixties to present the theoretical 1D ACPAR data in Si based on the band structure.[10] In their method they used empirical local pseudopotentials to obtain the electron wave functions, and experimental electron charge densities to obtain the positron wave function. Their theoretical data had an excellent agreement with experimental data. The 1D ACPAR data on Ge calculated with the electron wave functions obtained from the empirical nonlocal pseudopotentials and the positron wave function calculated in the frozen-core approximation also showed excellent agreement with the experimental data.[11] However, since the momentum distributions in diamond have not yet been calculated, the reason for the observed difference in 2D measurements cannot be understood.

Fujiwara and co-workers proposed a many-body theory for calculating the electron-positron interaction in a lowest-order ladder graph in a lattice on the basis of the two-band system.[12] From this theory it was concluded that there is an enhancement of the annihilation rate on the zone face, and that the high-momentum components are dehanced due to intraband and interband transitions, respectively. Comparison of the experimental 1D ACPAR data with theory based on the independent particle model approximation (IPM) of

Stroud and Ehrenreich confirmed this theoretical prediction.[12] In Ge this many-body effect was also studied, and a similar conclusion was arrived at.[11] Based on this picture Liu, Berko, and Mills suggested that the reason for the flattened momentum density in diamond is because the valence electrons are tightly bound to the nucleus, and do not participate to the same extent in the electron-positron interaction. We point out, however, that such explanations, in regard to the low-momentum regions of the momentum density, can at best be only one factor in explaining the complex fine structures found in Si and Ge. The reason for this is that the bonding mechanisms in the interstitial regions are also reflected in the low-momentum region of the momentum distributions, the different structures in the momentum distributions for a particular direction being ascribed to the nature of bonding in that direction.[13] For cubic semiconductors it has been shown that the valleys arise from the admixture of σ and π bonds, while the peaks are due to pure σ bonding. Therefore it must be concluded that the features in the low-momentum region are due to both the bonding mechanisms and the electron-positron many-body effects.

The present work, using the first-principles calculation, aims to see whether the vanishing of the structures in the momentum densities in diamond is due to band-structure effects or to correlation effects. To do this, a band-by-band momentum densities are calculated in diamond, Si, and Ge. This is because the band-by-band valence charge densities in Si computed in the pseudopotential theory have shown that the third and fourth bands are sp^3 hybridized and participate in bonding, whereas the first band is isotropic and the second band lies in between these two types. Comparison of the theoretical momentum density based on the IPM with the experimental momentum density will clearly separate the effect of the electron-positron interaction effects in diamond, Si, and Ge.

In Sec. II the method of calculating the ACPAR and momentum density is presented. In Sec. III the calculated 1D ACPAR will be compared with the available experimental data. The calculated momentum densities will be compared with the experimental data to bring out the electron-positron many-body correlation and the electron bonding features. In Sec. IV we summarize the conclusions of this work.

II. THEORY

The two-dimensional angular correlation data are expressed as[2]

$$N(p_x, p_y) = \int \rho^{2\gamma}(\mathbf{p}) dp_z, \qquad (2.1)$$

where the electron-positron momentum density is given by

$$\rho^{2\gamma}(\mathbf{p}) = \left(\frac{\pi r_0^2 c}{8\pi^3} \right) \sum_{n\mathbf{k}} \eta_{n\mathbf{k}} \left| \int e^{i\mathbf{p}\cdot\mathbf{r}} \Psi_{n\mathbf{k}}(\mathbf{r}) \right.$$
$$\left. \times \Psi_+(\mathbf{r}) \sqrt{\gamma_{n\mathbf{k}}(\mathbf{r})} d^3 r \right|^2. \qquad (2.2)$$

Here $\Psi_{n\mathbf{k}}(\mathbf{r})$ and $\Psi_+(\mathbf{r})$ are the occupied electron and positron wave functions, respectively, and $\eta_{n\mathbf{k}}$ is the occupation probability. $\gamma_{n\mathbf{k}}(\mathbf{r})$ describes both the distortion of the posi-

tron wave function from its initial shape and the enhancement of densities of individual electronic states on the positron site.[14] In the IPM approximation $\gamma_{n\mathbf{k}} = 1$. Although the form of $\gamma_{n\mathbf{k}}(\mathbf{r})$ is well known in metals, its form in semiconductors is not yet known. The individual core states lie deeply below the bottom of the conduction band. Therefore $\gamma_{n\mathbf{k}}(\mathbf{r})$ is replaced by $\gamma(\mathbf{r})$ for calculating the momentum density for core states. In the present work the contact density of Puska et al., which is applied to calculate the positron lifetime in various semiconductors, is used.[15] Gilgien et al. have used this $\gamma(\mathbf{r})$ for the valence electrons in Eq. (2.2) to calculate the electron-positron momentum density.[16]

The calculation of the electron and positron wave functions needs the complete many-body problem of interacting electron and positron treated in the two-component density-functional theory. In the present work a single positron in many-electron system is taken into account. For a delocalized positron the positron density is vanishingly small at every point of the infinite lattice,[17] so that the two-component density-functional theory reduces to the following practical scheme. The self-consistent electronic structure is first calculated without the positron, and then the electron charge density is used to calculate the long-range attractive electron-positron Coulomb potential and the short-range correlation potential.

We have used the *ab initio* pseudopotential technique in the momentum space formalism to calculate the electron wave functions. In this calculation, the norm-conserving ionic pseudopotentials of Bachelet, Hamann, and Schlüter are used.[18] The exchange-correlation potential is of Ceperley-Adler type, as parametrized by Perdew and Zunger.[19,20] The electron wave function can be described as

$$\Psi_{n\mathbf{k}}(\mathbf{r}) = \frac{1}{\sqrt{\Omega}} \sum_{\mathbf{G}} C_{n\mathbf{k}}(\mathbf{G}) e^{i(\mathbf{k}+\mathbf{G})\cdot\mathbf{r}}, \qquad (2.3)$$

where the symbols have their usual meanings.

The positron-ion potential is calculated in the frozen-core approximation, which considers a repulsive Coulomb potential term due to the nucleus and an attractive potential due to the core electrons.[21] Although this potential is divergent at the origin, the positron wave function can be represented by plane waves like the electron wave function because it has no oscillations in the ion core region. The electron-positron correlation potential is of Arponen-Pajanne type, as parametrized by Boronski and Nieminen.[22,23] We have also taken the factor arising from the band gap of the semiconductors.[15] The thermalized positron wave function is expressed as

$$\Psi_+(\mathbf{r}) = \frac{1}{\sqrt{\Omega}} \sum_{\mathbf{G}} D(\mathbf{G}) e^{i\mathbf{G}\cdot\mathbf{r}}. \qquad (2.4)$$

The two-photon momentum density in Eq. (2.2) in the IPM can be reexpressed in terms of Eqs. (2.3) and (2.4) as

$$\rho^{2\gamma}(\mathbf{p}) = \frac{1}{\Omega} \sum_{n\mathbf{k}} \eta_{n\mathbf{k}} \sum_{\mathbf{G}} \left| \sum_{\mathbf{K}} C_{n\mathbf{k}}(\mathbf{K}) D(\mathbf{G}-\mathbf{K}) \right|^2$$
$$\times \delta(\mathbf{p}-\mathbf{k}-\mathbf{G}). \qquad (2.5)$$

The positron wave function in the presence of the electron-positron correlation can be expanded like in Eq. (2.4) as

$$\Psi_+(\mathbf{r})\sqrt{\gamma(\mathbf{r})}=\frac{1}{\sqrt{\Omega}}\sum_\mathbf{G} D^{\text{enh}}(\mathbf{G})e^{i\mathbf{G}\cdot\mathbf{r}}. \qquad (2.6)$$

Traditionally the momentum density is either calculated directly from Eq. (2.5) or in the symmetry-related angular momentum components as done by Seth and Ellis.[24] In the present work we have adopted a recently developed scheme where the symmetry-related angular momentum components of the momentum density are calculated using electron and positron wave functions in the plane-wave expansion basis.[25,26] In this approach the autocorrelation function, which is the Fourier transform of the momentum density, is calculated first:

$$B^{2\gamma}(\mathbf{r})=\int \rho^{2\gamma}(\mathbf{p})e^{i\mathbf{p}\cdot\mathbf{r}}d^3p. \qquad (2.7)$$

Substituting Eq. (2.5) into Eq. (2.7), we obtain

$$B^{2\gamma}(\mathbf{r})=\frac{1}{\Omega}\sum_{n\mathbf{k}}\ \eta_{n\mathbf{k}}\sum_\mathbf{G}\ \left|\sum_\mathbf{K} C_{n\mathbf{k}}(\mathbf{K})D(\mathbf{G-K})\right|^2 e^{i(\mathbf{k+G})\cdot\mathbf{r}} \qquad (2.8)$$

For incorporating the enhancement factor into this expression, $D(\mathbf{G})$ is replaced by $D^{\text{enh}}(\mathbf{G})$. The factor $e^{i(\mathbf{k+G})\cdot\mathbf{r}}$ can be expanded in spherical harmonics as

$$e^{i(\mathbf{k+G})\cdot\mathbf{r}}=4\pi\sum_{lm}\ i^l j_l(|\mathbf{k+G}|r)Y_{lm}(\Omega_\mathbf{r})Y_{lm}^*(\Omega_\mathbf{k+G}). \qquad (2.9)$$

Substituting this into Eq. (2.8), we obtain

$$B^{2\gamma}(\mathbf{r})=\sum_{lm} B_{lm}^{2\gamma}(r)Y_{lm}(\Omega_r), \qquad (2.10)$$

where

$$B_{lm}^{2\gamma}(r)=\frac{4\pi}{\Omega}i^l\sum_{n\mathbf{k}}\ \eta_{n\mathbf{k}}\sum_\mathbf{G}\ \left|\sum_\mathbf{K} C_{n\mathbf{k}}(\mathbf{K})D(\mathbf{G-K})\right|^2$$
$$\times j_l(|\mathbf{k+G}|r)Y_{lm}^*(\Omega_\mathbf{k+G}) \qquad (2.11)$$

For including the enhancement factor into this expression, one needs to replace $D(\mathbf{G})$ by $D^{\text{enh}}(\mathbf{G})$ given in Eq. (2.6). Inversion of Eq. (2.7) yields

$$\rho^{2\gamma}(\mathbf{p})=\int B^{2\gamma}(\mathbf{r})e^{-i\mathbf{p}\cdot\mathbf{r}}d^3r. \qquad (2.12)$$

Expanding $e^{-i\mathbf{p}\cdot\mathbf{r}}$ in a similar manner that in Eq. (2.9), and substituting in Eq. (2.12), we obtain

$$\rho^{2\gamma}(\mathbf{p})=\sum_{lm} \rho_{lm}^{2\gamma}(p)Y_{lm}(\Omega_\mathbf{p}), \qquad (2.13)$$

where

$$\rho_{lm}^{2\gamma}(p)=4\pi(-i)^l\int_0^\infty B_{lm}^{2\gamma}(r)j_l(qr)r^2dr. \qquad (2.14)$$

In this calculation cubic harmonic functions consistent with the O_h group are used. Following Mueller and Priestley,[27]

the cubic harmonic function is expressed as a linear combination of spherical harmonic functions as

$$K_l^i=a_{l0}^i Y_{l0}+\sum_{m=1}^l a_{lm}^i\frac{1}{\sqrt{2}}(Y_{lm}+Y_{l-m}), \qquad (2.15)$$

where i distinguishes the various irreducible representations for a specific value l.

Like the two-dimensional angular correlation data described in Eq. (2.1), the one-dimensional angular correlation data are given by

$$N(p_z)=\int\int \rho^{2\gamma}(\mathbf{p})dp_x dp_y=2\pi\sum_{li}\ g_{li}(p_z)K_l^i(\beta,\alpha), \qquad (2.16)$$

where

$$g_{li}(p_z)=\int_0^\infty \rho_{li}(\mathbf{p})P_l(p_z/p)dp_z, \qquad (2.17)$$

The core momentum density can be calculated replacing the Bloch wave function by the free-atom wave function in Eq. (2.2), which will take the form

$$\rho^c(\mathbf{p})=\left(\frac{\pi r_0^2 c}{8\pi^3}\right)\sum_i\ \lambda_i\left|\int \Psi_i(\mathbf{r})\Psi_+(\mathbf{r})e^{i\mathbf{p}\cdot\mathbf{r}}d^3r\right|^2, \qquad (2.18)$$

where the summation is over all different core states. One can notice that we have taken a factor λ_i which represents the partial positron annihilation rate. This factor was recently used by Alatalo et al. to account for the proper weights of the contribution of each orbital:[28]

$$\lambda_i=\int \rho_+(\mathbf{r})\gamma(\mathbf{r})\frac{\rho_i(\mathbf{r})}{\rho(\mathbf{r})}d\mathbf{r}. \qquad (2.19)$$

In this equation $\rho(\mathbf{r})$ and $\rho_+(\mathbf{r})$ represent electron and positron densities, respectively. In the IPM approximation λ_i is taken to be unity. We have taken the free-atomic orbitals of Clementi and Roetti in this calculation.[29]

We have taken the lattice constants of diamond, Si, and Ge to be 3.56, 5.431, and 5.65 Å, respectively. For both positron and electron wave functions in Si and Ge, 600 plane waves have been taken, while for diamond 800 plane waves were found necessary. The $\mathbf{k}$ summation was carried out in the special point scheme of Chadi and Cohen using 60 points.[30]

The momentum density without any core contributions has a sharp cutoff at the Jones zone face, whereas the momentum distribution, whether calculated for 1D or 2D ACPAR methods, falls slowly. As a result of the sharp drop it is not a straightforward task to obtain $\rho_{lm}^{2\gamma}(\mathbf{p})$ from the Fourier-Bessel transform method, because outside the zone face region there will exist unphysical auxiliary oscillations in the momentum density. These oscillations depend very much on the range of r taken in the Fourier-Bessel transformation, and with appropriately large r values the oscillations can be minimized, but never reduced identically to zero at high moments. An optimal procedure here is to use a nonnegativity constraint in the Fourier-Bessel transform so as to obtain the appropriate momentum density. In the present
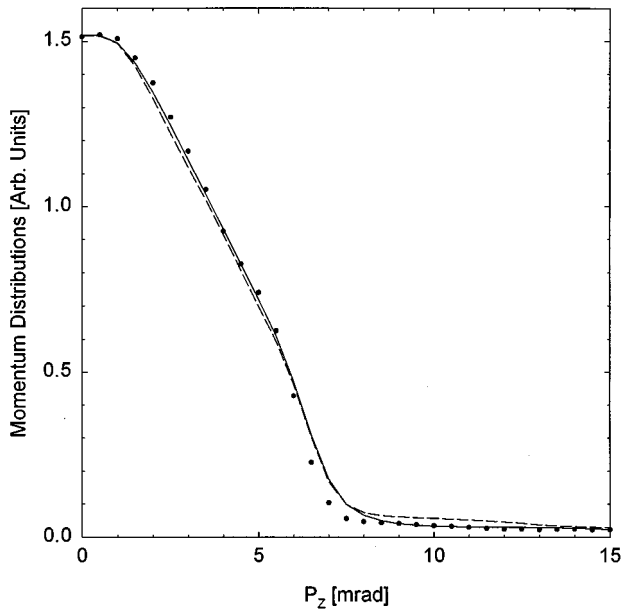
FIG. 1. Experimental and theoretical 1D ACPAR along the [110] direction of Si. The solid and dashed curves represent the theory with and without inclusion of correlation effects, respectively, while the experimental data of Fujiwara and Hyodo are shown by solid dots.

work we have used the range of r in all $B_{lm}^{2\gamma}(r)$ calculations to be 51 a.u., with 0.1 a.u. steps, and found that the oscillations are small enough to be negligible. The total momentum density is a combination of angular-momentum-dependent momentum densities $\rho_{lm}^{2\gamma}(\mathbf{p})$, and needs a convergence test as far as the number of angular momenta taken into consideration is concerned. From our experience we have found that
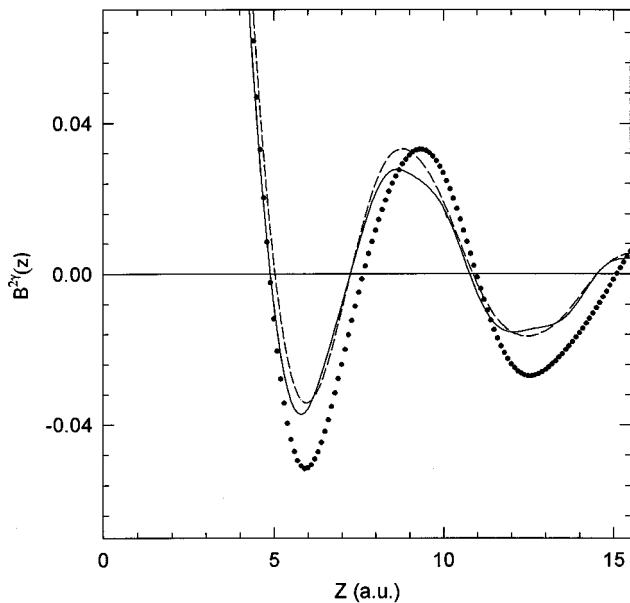

FIG. 2. Experimental and theoretical two-photon autocorrelation function along the [110] direction of Ge. The solid and dashed curves represent the theory with and without inclusion of correlation effects, respectively, while the experimental data of Fujiwara and Hyodo are shown by solid dots.
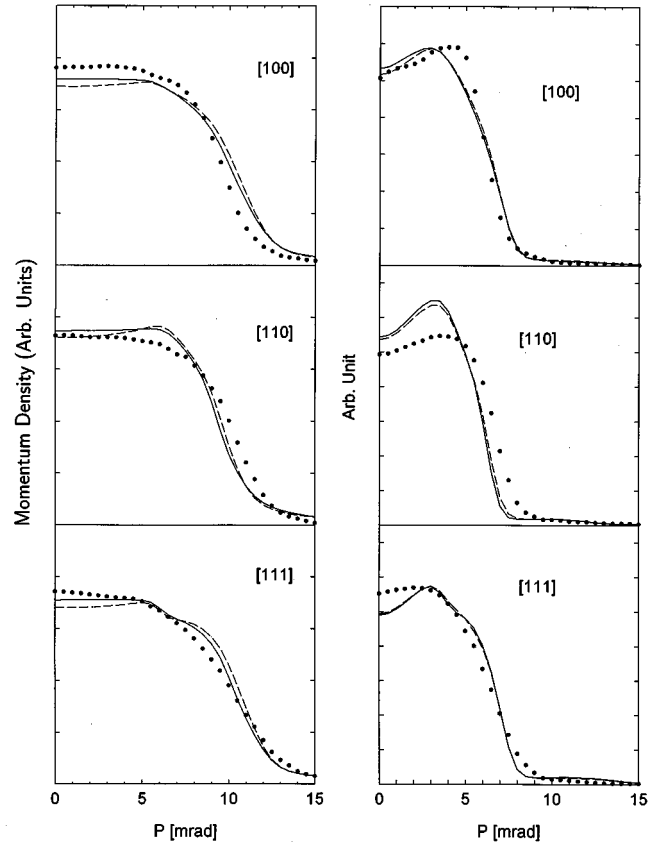

FIG. 3. Experimental and theoretical momentum densities projected along the [100], [110], and [111] directions in diamond (left) and Ge (right). The solid and dashed curves represent the theory with and without inclusion of correlation effects, respectively, while the experimental data of Liu, Berko, and Mills are shown by solid dots.

the first four angular momentum components (l=0, 4, 6, and 8) are sufficient to reconstruct the total momentum densities in all cases.

The theoretical and experimental 1D ACPAR data are normalized to unity for comparison. The theoretical valence and core momentum densities along different crystal directions are added, and then both the theoretical and experimental momentum momentum density data are normalized to unity for comparison.

III. RESULTS AND DISCUSSIONS

The electron-positron correlation effect is seen most clearly along the [110] direction, with the zone face pointing in this direction. Thus, in general, along this direction there is a drop in the momentum distribution.[4] Comparison of the theoretical 1D ACPAR data calculated in the IPM approximation with the experimental data at the zone face reveals the electron-positron enhancement effect.[12] However, some precautions are necessary to preserve this information in the experimental data while taking measurements. Specifically the sharp slope in the momentum distribution at the zone face is both smeared by the convolution of the angular resolution of the spectrometer and the positron thermal motion. In order to avoid these problems Fujiwara and Hyodo took a
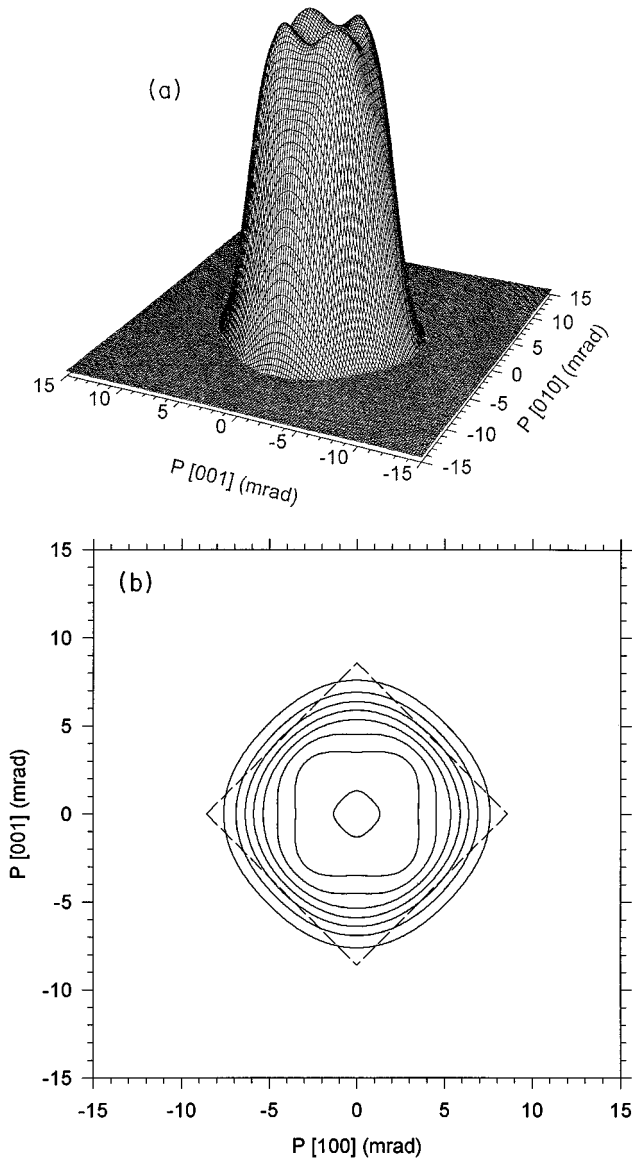
FIG. 4. Calculated momentum densities and the countermap in Ge with the normal along the [010] direction. The dashed line denotes the Jones zone.
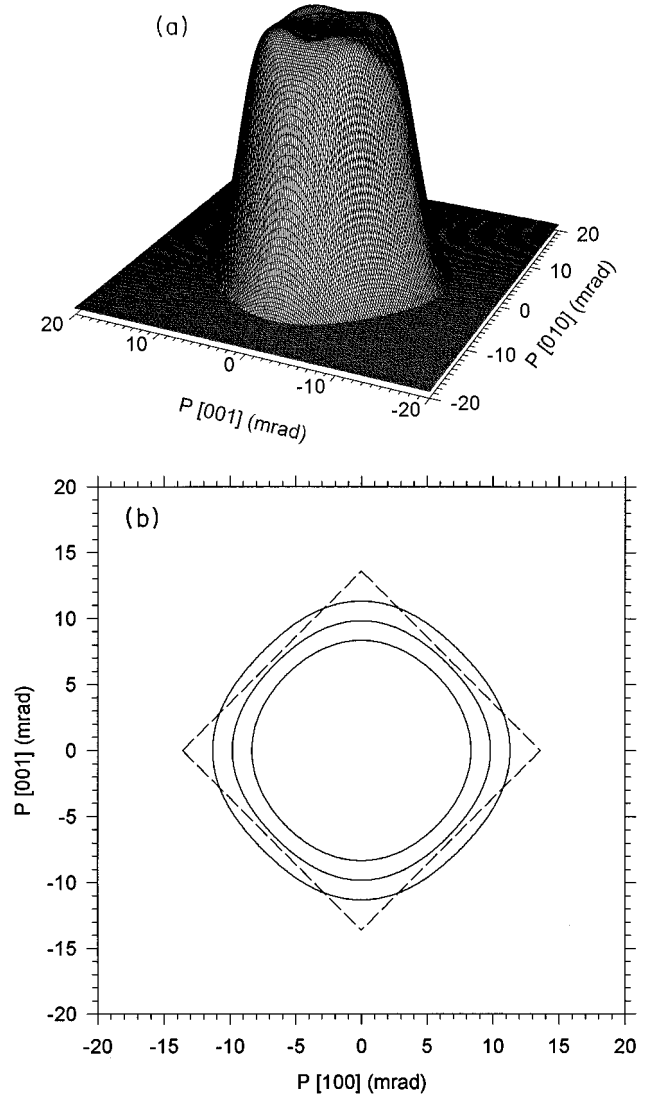

FIG. 5. Calculated momentum densities and the countermap in diamond with the normal along the [010] direction. The dashed line denotes the Jones zone.

high-resolution 1D ACPAR measurement at low temperature to see the effect of electron-positron enhancement at the zone face.[12] These authors compared their data with the local pseudopotential theory of Stroud and Ehrenreich,[10] in which core contributions were not included. Since our calculation, based as it is on the *ab initio* method, contains all known physical interactions together with the electron-positron enhancement factor, it is worthwhile comparing our theory with the experimental data. The unit-normalized 1D ACPAR data calculated with and without the correlation effect are presented in Fig. 1 together with the unit-normalized experimental data of Fujiwara and Hyodo. The theory is seen to reproduce the main features of the experimental data well with the inclusion of correlation effects, showing better agreement with the experimental data in the low-momentum region. Of great interest is the observation that in the high-momentum region the calculation without correlation effects reveals a departure of the theory from the experiment at the

high-momentum region due to the dehancement effect. However, when correlation effects are included, the agreement between experiment and theory in this region is excellent, confirming the dehancement of the core momentum distribution. With regard to the momentum distribution at the zone face the agreement is not good, showing the same fall with and without the enhancement factor. This indicates that the enhancement prescription of Gilgien *et al.* is not appropriate for valence electrons. Finally we note that our theory does not explain the small hump seen at 9.5 mrad in the experimental data which is attributed to the positron-ion interaction by Arutyunov.[6]

The other method of looking at the enhancement effect is to verify the zero positions of the autocorrelation function along the [110] direction. It is known that the data based on the IPM approximation show zero positions exactly at the lattice points, while the same for the experimental data are shifted to the right.[31,11] In Fig. 2 two-photon autocorrelation data are presented for our present theory and the experimental data of Fujiwara and Hyodo.[12] We once again observe
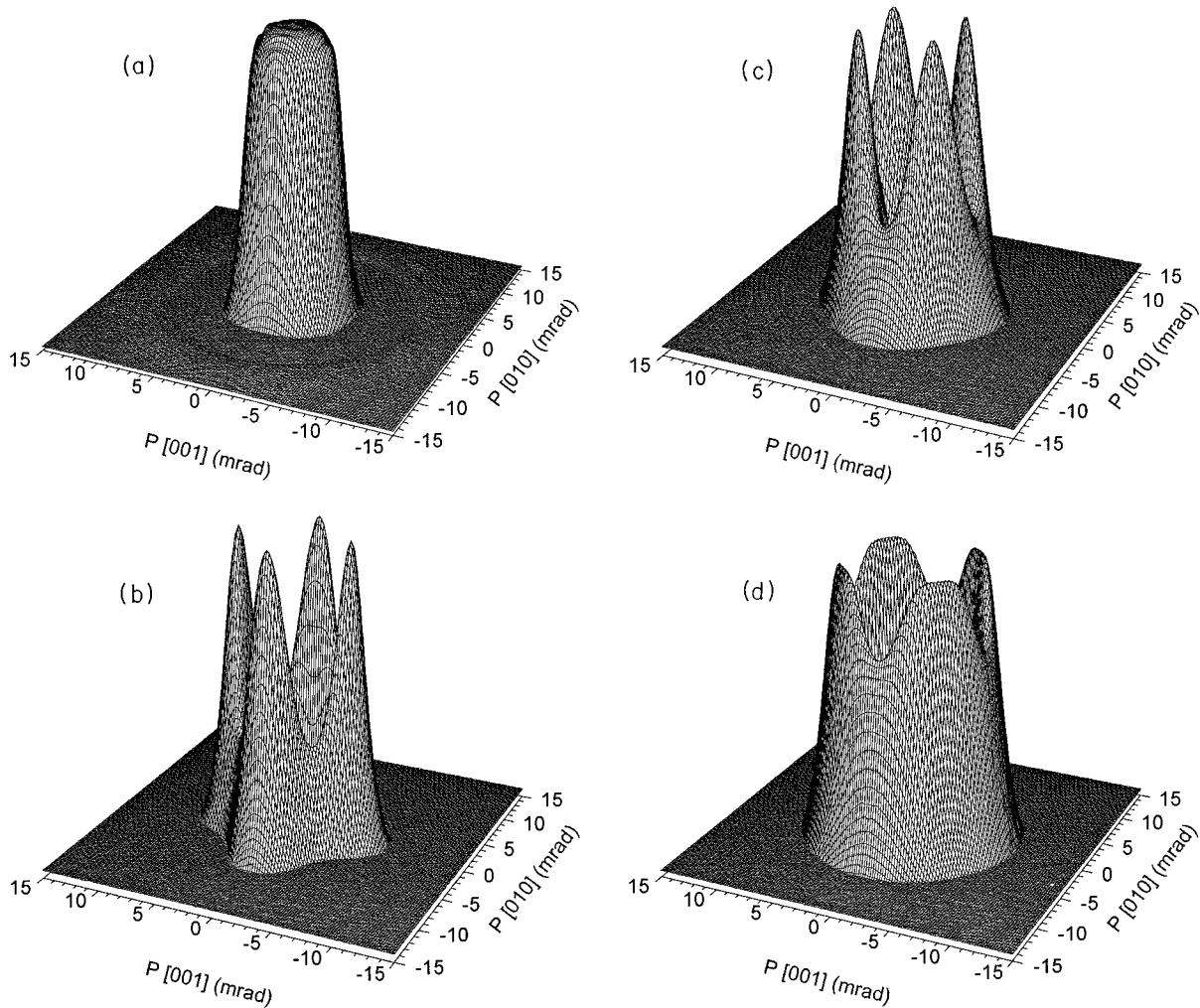
FIG. 6. Calculated momentum densities in Ge with the normal along the [100] direction for the first, second, and fourth bands.

that the zero positions in the experimental data are shifted to the right, and more importantly that the theoretical data with and without the correlation effect as prescribed by Gilgien *et al.* show the same zero positions.

In ACPAR studies the momentum density is always integrated along some crystal axes, and the detailed nature of the correlation effects is consequently lost when a comparison is made between theoretical and experimental data. Therefore, in Fig. 3 we have compared our theory with the experimental momentum densities for diamond and Ge along the [100], [110], and [111] projections as obtained by Liu, Berko, and Mills.[9] In both diamond and Ge, along all projections the theoretical data with correlation effects show slightly more momentum broadening than without correlation effects. It is noted that in Ge both theory and experiment show significant dips in the low-momentum regions for the [100] and [110] projections, whereas in contrast the experimental data along the [111] projection show no dip, in disagreement with theory where one is present. Another remarkable feature is that the momentum broadening in the experimental data along [100] and [111] projections for both diamond and Ge is less than that predicted by theory, while the exact opposite pertains to the [110] projection. Figure 3 also reveals an important difference between diamond and Ge, in that both the experimental and theoretical data for diamond show no dip

in the low-momentum region; we shall comment on this below. The higher-momentum broadening in diamond compared to Ge is simply understood in terms of the smaller lattice constant. Surprisingly, however, in diamond with its simpler core contribution, the mismatch between theory and experiment is more prominent in the high-momentum region than in Ge. It is interesting to note from Fig. 3 that the core contributions is isotropic neither in diamond nor in Ge, a fact that is difficult to explain on any theoretical basis, and which we ascribe to a possible systematic error in the experimental data of the high-momentum region. A notable difference between the momentum density data of Tanigawa (cf. Fig. 6 of Ref. 8) strengthens the view that systematic errors are present in the data of Liu, Berko, and Mills. From the above observation of the 1D and 2D ACPAR data, it is clear that the present calculation cannot explain the sharpness of the momentum density. The simple conclusion is that the enhancement factor of Gilgien *et al.* cannot be applied to valence electrons is semiconductors. As a final point we mention that for diamond the theoretical data without the enhancement factor also have a flat top as in the experimental data suggesting, that the electron-positron correlation effect for valence electrons is not so important in diamond because the electrons are more tightly bound. Calculations of the effect of the correlation potential on the wave function and the
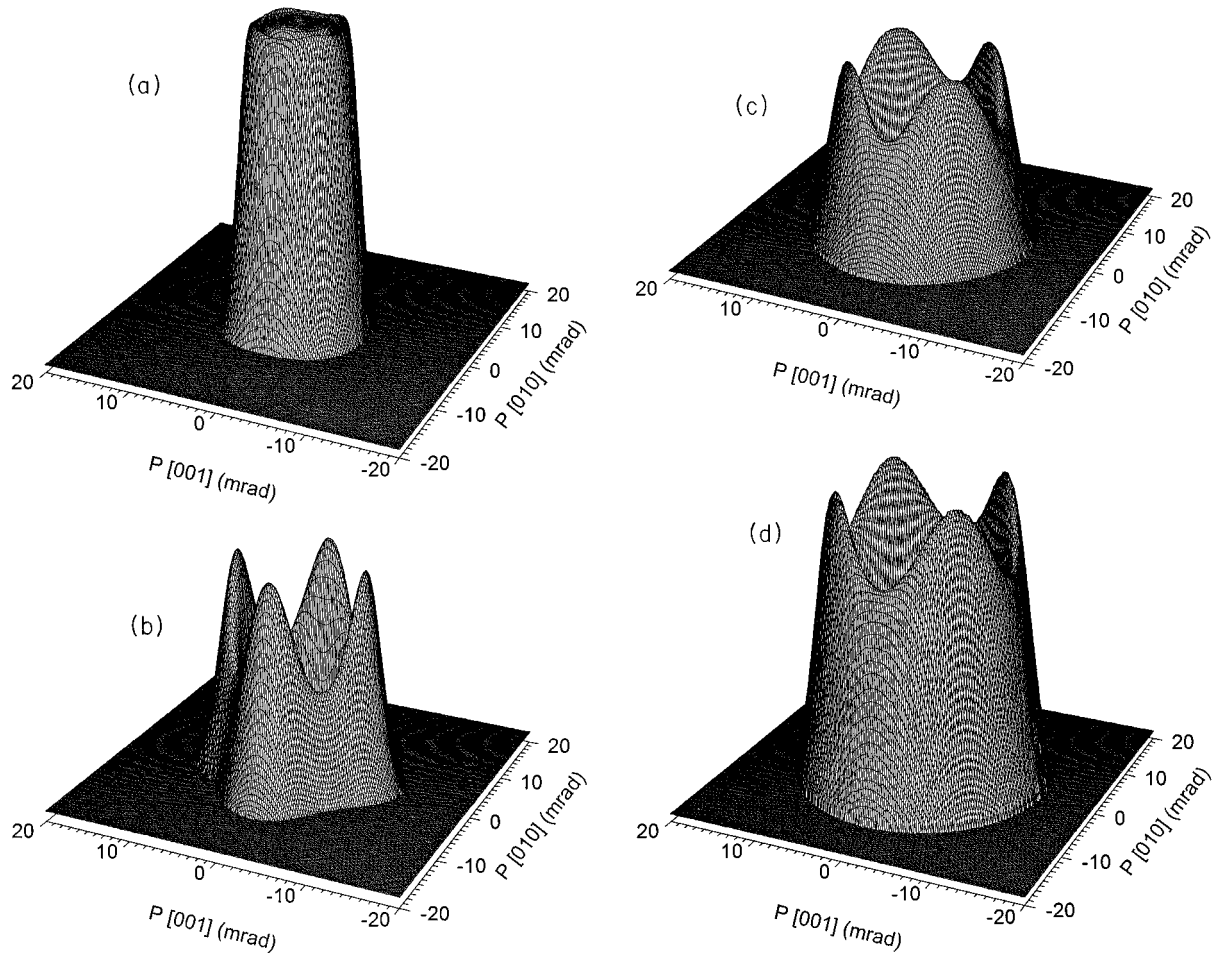
FIG. 7. Calculated momentum densities in diamond with the normal along the [100] direction for the first, second, third, and fourth bands.

positron lifetimes in diamond, Si, and Ge also show that the effect of correlation on diamond is much smaller than on Si and Ge.[32]

With regard to the structure of the momentum density in the low-momentum region, Chiba and Akahane in their linear combination of the atomic orbitals (LCAO) calculation noted that the upper three bands are mainly p states, and have suggested this will lead to the inversion of orbitals in the nearest-neighboring sites, the momentum density from two sites canceling each other and contributing very little to the total momentum density.[33] Saito, Oshiyamo, and Tanigawa, exploiting this idea, were able to explain the structure of the peak positions in the momentum density using group-theoretical methods.[34] We point out here, however, that the same reasoning would also lead to the expectation of such peaks being present in diamond, where experimentally they are not observed. Although we have not been able to take the correlation effects for the valence electrons correctly into account in our calculations, we have successfully obtained structures at the peak in the momentum density data, and this leads to a much clearer interpretation arising in terms of the electron bonding.

We show the momentum density plot for both Ge and diamond in Figs. 4 and 5, respectively. These plots are to be compared with the experimental data of Liu, Berko, and Mills[9] and Tanigawa (cf. Fig. 6 of Ref. 8). It may be seen

that although our calculations do not explain the detailed structure of the experimental data, they do correctly give the dip and valley structures found at the peak in Ge and flat top in diamond. In order to understand this, in Fig. 6 we have plotted for Ge the contributions from each band to the momentum density. From this figure the first band is seen to be isotropic, and cannot contribute to the observed structure. Furthermore, while the second band has low momentum peaks, they are directed in the [100] direction, and thus we conclude that this band also does not contribute to the observed structure. The third and fourth bands are the only ones that contribute to the shape of the features seen at the low-momentum region in the momentum density data. Figure 7 shows the contributions from each band in diamond. The same general picture emerges of the first band being isotropic, the second band being symmetric about the [100] direction, and the third and fourth bands exhibiting symmetry about the [110] direction. However, the structures are much weaker than for Ge, giving an overall flat isotropic momentum density.

The above structures seen in the third and fourth bands of both Ge and diamond are easily understood by considering the nature of the bonding, the latter having a strong influence on the low-momentum region of the electron momentum density. In cubic semiconductors it has been shown that there is a (p,p) bond at the first bond length, and that the interac-

FIG. 9. The momentum density at the [100] projection for diamond and Ge calculated at the lattice constant of 3.56 Å.
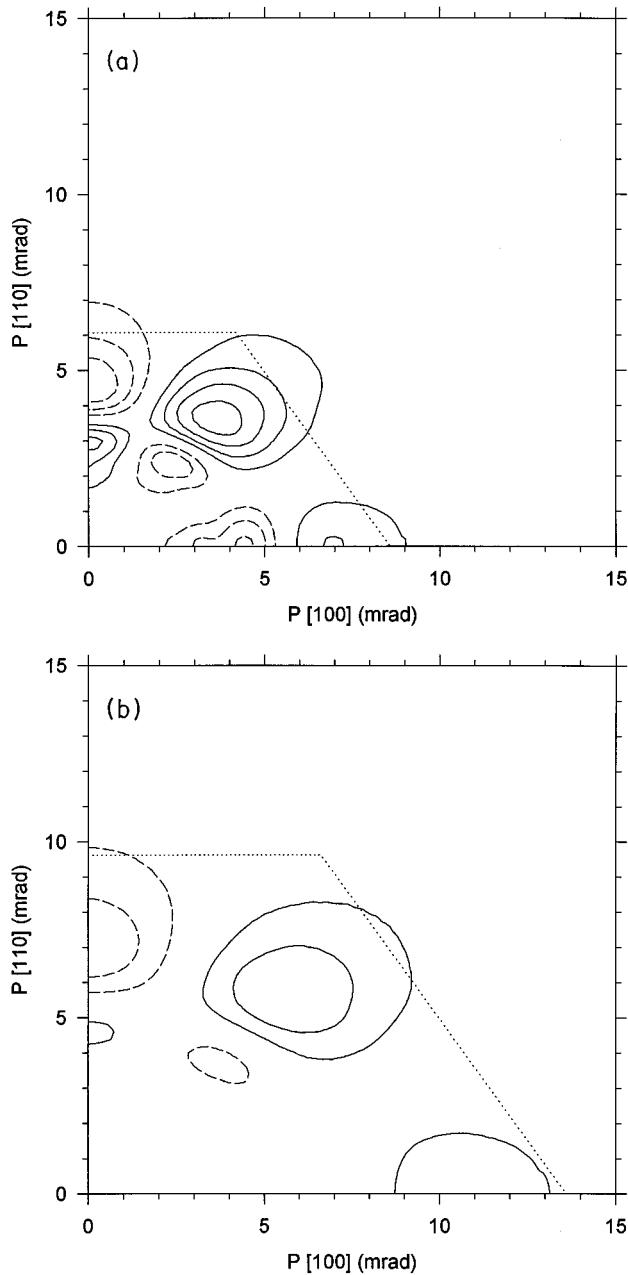

FIG. 8. Calculated anisotropic momentum densities in Ge (left) and diamond (right) are shown with positive and negative contours denoted by solid and dashed lines, respectively. The dotted line denotes the Jones zone.

tion of the second-neighbor (p,p) bonds is equivalent to introducing a $(p,p)\pi^*$ bond between neighboring atoms.[35] As a result of this there is a strong $(p,p)\sigma$ bond along the [111] direction, and an admixture of $(p,p)\sigma$ and $(p,p)\pi^*$ bonds along the [110] directions. Pattison, Hansen, and Schneider have shown that in the anisotropic 3D autocorrelation function in diamond and Si Compton profile data there is a dip at the first bond length along the [111] direction due to the $(p,p)\sigma$ bond, and a peak at the second bond length along the [110] direction due to the $(p,p)\pi$ bond.[36] Since the momentum density is obtained as a Fourier transform of the 3D autocorrelation function, the dip along the [111] direction becomes a peak, and the peak along the [110] direction be-
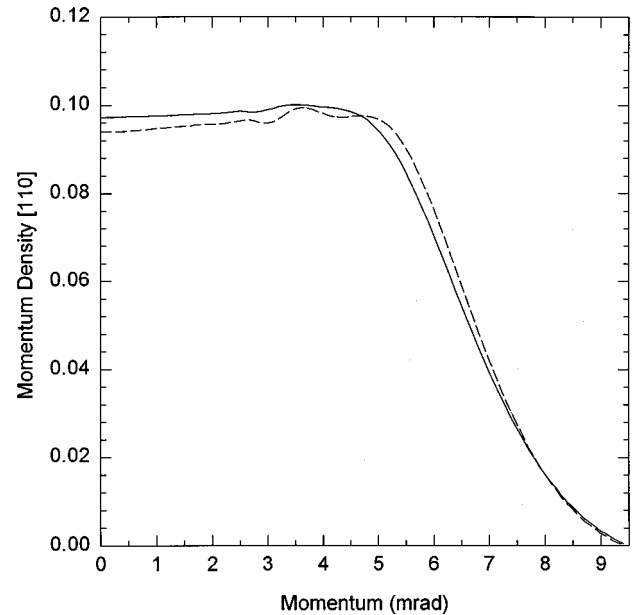
comes a dip. We have obtained the anisotropic momentum density data by dropping the $l=0$ contribution in Eq. (2.13), and show in Fig. 8 the contour plots of the momentum densities in Ge and diamond. As expected, the peak and dip positions are seen both in Ge and diamond. However, the small lattice constant in diamond causes a much stronger overlap of the sp^3 orbitals compared to Ge, so that in momentum space the diamond data show a more diffused behavior than in Ge.

Recently Benkabou *et al.* have calculated pressure-dependent electron-positron momentum densities in Si, and found that with decreasing lattice spacing the momentum densities become flattened at the top.[37] The reduction in the lattice constant expands the momentum distribution and thus affects the peak positions of the momentum density. The bonding strengths of the σ and π bonds also change significantly. These two changes combine to alter the shape of the momentum density data. To illustrate the effect of lattice spacing, in Fig. 9 we have shown the momentum density in the [110] direction, with the lattice constant of Ge replaced by that of diamond. In the same figure we have also plotted the momentum density of diamond. From this comparison it is clear that the momentum density of Ge has a greater momentum spread than that of diamond, indicating that simple lattice scaling is not strictly valid. Moreover, the momentum density in Ge shows oscillations which arise from the fact that the lattice constant of Ge cannot be reduced to such a small value without the crystal structure changing.[38] Nevertheless an important conclusion is drawn that the present calculation shows that with a compressed lattice constant the dip at the low-momentum region in the momentum density vanishes. The flattening in the peak in diamond might arise from its small lattice constant.

IV. CONCLUSION

In this work the momentum densities of diamond and Ge and the 1D ACPAR of Si are carried out. The 1D ACPAR

shows that the enhancement factor as proposed by Gilgien *et al.* is not correct. However, for core electrons this is a correct method. The analysis shows that the electron-positron enhancement effect is quite necessary to explain the sharpness of the momentum densities. Unfortunately such a formula does not exist at present, and is very much required to formulate a formula because there are currently much activity in momentum distribution studies. Detailed studies of the enhancement factor in metals have shown that both the density parameter r_s and the electron energies $E_{n\mathbf{k}}$, above the conduction-band minimum are important. For semiconductors a third parameter, such as the band-gap parameter or ϵ_∞ as used in the lifetime analysis, has to be included in one formula to calculate the enhancement factor. We point out

that the core-orthogonalization effect which is neglected in our calculation is not so important for the momentum density studies, because the positron avoids the core region. The vanishing of the dip in diamond could arise from its small lattice constant and weak electron-positron interaction. Work is in progress to separate the effect of the ionic bond on the momentum density in compound semiconductors.

ACKNOWLEDGMENTS

[1] For example, see M. L. Cohen and J. R. Chelikowsky, in *Electronic Structure and Optical Properties of Semiconductors*, edited by M. Cardona (Springer-Verlag, Berlin, 1988).

[2] For example, see S. Berko, in *Positron Solid State Physics*, edited by W. Brandt and A. Dupasquire (North-Holland, Amsterdam, 1983), p. 64.

[3] P. Colombino, B. Fiscella, and L. Trossi, Nuovo Cimento **31**, 950 (1964).

[4] J. C. Erskine and J. D. McGervey, Phys. Rev. **151**, 615 (1966).

[5] M. A. Shulman, G. M. Beardsley, and S. Berko, Appl. Phys. **5**, 367 (1975).

[6] N. Y. Arutyunov, Mater. Sci. Forum **105–110**, 583 (1992).

[7] R. N. West, J. Mayers, and P. A. Walters, J. Phys. E **14**, 478 (1981).

[8] S. Tanigawa, Mater. Sci. Forum **105–110**, 493 (1992).

[9] W. Liu, S. Berko, and A. P. Mills, Jr., Mater. Sci. Forum **105–110**, 743 (1992).

[10] D. Stroud and H. Ehrenreich, Phys. Rev. **171**, 399 (1968).

[11] B. K. Panda and D. P. Mahapatra, J. Phys. Condens. Matter **5**, 3475 (1993).

[12] K. Fujiwara, T. Hyodo, and J. Ohyama, J. Phys. Soc. Jpn. **33**, 1047 (1972), K. Fujiwara and T. Hyodo, *ibid.* **35**, 1133 (1973).

[13] B. K. Panda, Phys. Rev. B **49**, 2521 (1994).

[14] S. Daniuk, M. Sob, and A. Rubaszek, Phys. Rev. B **43**, 2580 (1991).

[15] M. J. Puska, S. Mäkinen, M. Manninen, and R. M. Nieminen, Phys. Rev. B **39**, 7666 (1989).

[16] L. Gilgien, G. Galli, F. Gygi, and R. Car, Phys. Rev. Lett. **72**, 3214 (1994).

[17] M. J. Puska and R. M. Nieminen, Rev. Mod. Phys. **66**, 841 (1994).

[18] G. B. Bachelet, D. R. Hamann, and M. Schlüter, Phys. Rev. B **26**, 4199 (1982).

[19] D. M. Ceperley and B. J. Adler, Phys. Rev. Lett. **45**, 566 (1980).

[20] J. P. Perdew and Z. Zunger, Phys. Rev. B **23**, 5048 (1981).

[21] C. Pennetta and A. Baldereschi, in *Positron Annihilation*, edited by L. Dorikens-Vanpraet, M. Dorikens, and D. Segers (World Scientific, Singapore, 1988), p. 693.

[22] J. Arponen and E. Pajanne, Ann. Phys. (N.Y.) **121**, 343 (1979).

[23] E. Boronski and R. M. Nieminen, Phys. Rev. B **34**, 3820 (1986).

[24] A. Seth and D. E. Ellis, J. Phys. C **10**, 181 (1977).

[25] H. Nara, T. Kobayashi, K. Takegahara, M. J. Cooper, and D. N. Timms, Comput. Mater. Sci. **2**, 366 (1994).

[26] T. Kobayashi and H. Nara, Mater. Sci. Forum **175–178**, 903 (1995).

[27] F. M. Mueller and M. G. Priestley, Phys. Rev. **148**, 638 (1966).

[28] M. Alatalo, H. Kauppinen, K. Saarinen, M. J. Puska, J. Mäkinen, P. Hautojärvi, and R. M. Nieminen, Phys. Rev. B **51**, 4176 (1995).

[29] E. Clementi and C. Roetti, At. Data Nucl. Data Tables **14**, 177 (1974).

[30] D. J. Chadi and M. L. Cohen, Phys. Rev. B **8**, 5747 (1973).

[31] S. Berko, W. S. Farmer, and F. Sinclair, in *Positron Annihilation*, edited by P. G. Coleman, S. C. Sharma, and L. M. Diana (North-Holland, Amsterdam, 1981), p. 319.

[32] H. Rojas, B. Barbiellini, and T. Jarlborg, Mater. Sci. Forum **105–110**, 799 (1992).

[33] T. Chiba and T. Akahane, in *Positron Annihilation*, edited by L. Doriken-Vanpraet, M. Dorikens, and D. Seegers (World Scientific, Singapore, 1989), p. 674.

[34] M. Saito, A. Oshiyama, and S. Tanigawa, Phys. Rev. B **44**, 10 601 (1991).

[35] S. T. Pantelides and W. A. Harrison, Phys. Rev. B **11**, 3006 (1975).

[36] P. Pattison, N. K. Hansen, and J. R. Schneider, Chem. Phys. **59**, 231 (1981).

[37] F. Benkabou, J. P. Dufour, B. Soudini, N. Amrane, B. Khelifa, and H. Aourag, Phys. Status Solidi B **184**, 355 (1994).

[38] A. Mujica and R. J. Needs, Phys. Rev. B **48**, 17 010 (1993); M. Hebbache, *ibid.* **49**, 6522 (1994).